

Ultrathin SiO₂ on Si

II. Issues in quantification of the oxide thickness

M. P. Seah* and S. J. Spencer

Centre for Optical and Analytical Measurement, National Physical Laboratory, Teddington, Middlesex TW11 0LW, UK

Received 25 March 2002; Revised 8 May 2002; Accepted 8 May 2002

An analysis is made of various quantification issues concerning the analysis of ultrathin layers of SiO₂ on (100) and (111) polished Si surfaces. For analysis of the oxide thickness, a simple equation is generally used involving two parameters; the attenuation length of photoelectrons in the oxide and the ratio, R_o , of the intensities of the Si 2p peak from bulk thermal SiO₂ and from pure Si. An analysis of previously reported measurements of the attenuation length gives an average value of only 6% less than the theoretical value. However, careful measurements of R_o , via two routes, indicate consistently that a value of 0.88 ± 0.03 should be used rather than the calculated value of 0.53 ± 0.05 . This difference may arise through systematic uncertainties in the values for the relevant inelastic mean free paths, the silicon dioxide density and the shake-up contributions. Previously reported experimental values of R_o range from 0.67 to 0.87. Uncertainties also arise from intensity variations caused by the crystal structure of the substrate. These are mapped and a position 'A' is found where further work is best conducted. For the (100) surface, A is 34° from the surface normal in an azimuth midway at 22.5° between the [010] and [011] azimuths. For the (111) surface at A is 25.5° from the surface normal in the [10 $\bar{1}$] azimuth. Data for much of the present work are for the (100) surface at an angle of emission of 27° at position 'B' at 28.5° from the surface normal in the [110] azimuth, which is equivalently good but may degrade for spectrometers with high angular resolution. If the same equation is used for calculating the thickness, position B leads to a calculated thickness that is 4% less than that measured for an average orientation, whereas data acquired for normal emission lead to a value 18% lower, and those measured at A are 2% higher. Measurements of the carbonaceous contamination confirm earlier conclusions that the contamination is better described using data for an average polymer than for glassy carbon. © Crown Copyright 2002 Published by John Wiley & Sons, Ltd.

KEYWORDS: attenuation lengths; forward focusing; gate oxide; layer thickness; quantification; silicon; silicon oxide; XPS

INTRODUCTION

Measurement of the thickness of ultrathin SiO₂ layers on Si is very important and has been the subject of a wealth of published papers. Measurements in industry are often made using ellipsometry because it is particularly rapid and has extremely high precision. For thicknesses of >10 nm, ellipsometry has been the favoured method. Unfortunately, ellipsometry is sensitive to contamination layers at the surface and these become important for thickness measurements in the range 1–10 nm. However, this is precisely the range in which x-ray photoelectron spectroscopy (XPS) works well. Being an analytical technique, XPS should be able to measure oxide thickness irrespective of the contamination, and this is the focus of the present work.

In a previous paper in this series,¹ we have analysed the carbonaceous contamination that accretes on the oxide layer and have established simple methods to minimize

it. In the present work we consider the issues underlying quantification of the oxide thickness in order to clarify the measurements needed to obtain an optimum result.

ANALYSIS OF THE LAYERS BY XPS

We consider a model of the surface (as shown in Fig. 1) of a silicon single-crystal substrate with an overlayer of silicon dioxide of thickness d_{SiO_2} . On the surface is a contamination layer of thickness d_c and, at the silicon dioxide/silicon interface, various layers of intermediate oxides $d_{\text{Si}_2\text{O}_x}$, where $x = 1, 2$ or 3.

The thicknesses of the intermediate oxides are small and here we shall simply add them into a total oxide thickness of d_{oxide} , which is somewhat larger than the thickness of the SiO₂ layer, d_{SiO_2} , by approximately $0.25d_{\text{Si}_2\text{O}} + 0.5d_{\text{SiO}} + 0.75d_{\text{Si}_2\text{O}_3}$. These interfacial oxides need to be measured separately by peak synthesis in XPS and calculations of those amounts require full treatment as a direct extension of the treatment described in the present work for the SiO₂ overlayer. We do not do this separately here because, at this stage, more general considerations are important.

*Correspondence to: M. P. Seah, Centre for Optical and Analytical Measurement, National Physical Laboratory, Teddington, Middlesex TW11 0LW, UK. E-mail: martin.seah@npl.co.uk

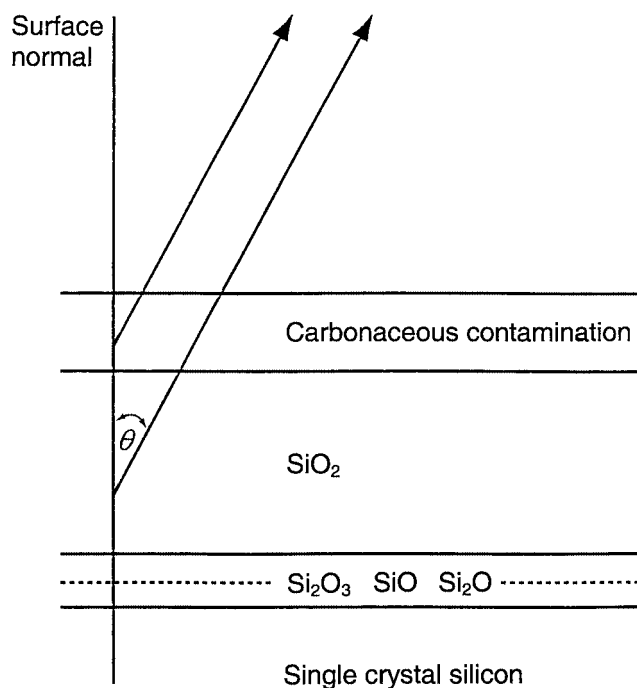


Figure 1. Schematic of the structure of the contamination and oxide layers analysed.

It is easiest first to consider the oxide thickness by measuring the intensities of the Si 2p peak area in the oxide and metallic states, I_{SiO_2} and $I_{\text{Si}_{\text{met}}}$, respectively. Thus, because these photoelectrons have very similar energies, using the results of inelastic and elastic scattering theory for XPS gives

$$\frac{I_{\text{SiO}_2}}{I_{\text{Si}_{\text{met}}}} = \frac{I_{\text{SiO}_2}^{\infty}}{I_{\text{Si}_{\text{met}}}^{\infty}} \frac{1 - \exp[-d_{\text{oxide}}/L_{\text{SiO}_2}(E_{\text{Si}}) \cos \theta]}{\exp[-d_{\text{oxide}}/L_{\text{SiO}_2}(E_{\text{Si}}) \cos \theta]} \quad (1)$$

where $I_{\text{SiO}_2}^{\infty}$ and $I_{\text{Si}_{\text{met}}}^{\infty}$ are the equivalent intensities for the pure bulk materials. The parameter $L_{\text{SiO}_2}(E_{\text{Si}})$ is the attenuation length for the Si 2p photoelectrons in SiO₂ and θ is the angle of emission of the detected electrons from the surface normal. Equation (1) may be simplified to give

$$d_{\text{oxide}} = L_{\text{SiO}_2}(E_{\text{Si}}) \cos \theta \ln(1 + R_{\text{expt}}/R_0) \quad (2)$$

where R_{expt} is the measured ratio $I_{\text{SiO}_2}/I_{\text{Si}_{\text{met}}}$ and R_0 is the ratio $I_{\text{SiO}_2}^{\infty}/I_{\text{Si}_{\text{met}}}^{\infty}$. Equation (2) is the basis equation for many studies of the oxide thickness on Si or, alternatively, of $L_{\text{SiO}_2}(E_{\text{Si}})$ from data for d_{oxide} . We shall return to these studies later in this section. One small approximation that we have used above is to ignore the fact that the oxide silicon electrons travelling through the oxide have 4.0 eV lower energy than those for the metallic state. This leads to an underestimation of the oxide thickness by $\sim 0.26\%$ from Eqn (2). We shall see later that there are more significant errors than this and so we shall ignore this effect for now.

There are two parameters, therefore, needed for deducing the oxide thickness from Eqn (2) from the measured intensity ratio R_{expt} . These parameters, R_0 and $L_{\text{SiO}_2}(E_{\text{Si}})$, have values that are thought to be effectively instrument independent and thus provide d_{oxide} values in any XPS instrument without the need for any calibration. We assess the current knowledge of these parameters below. We then describe experimental

results that provide a value for R_0 and a basis for more accurate determination of $L_{\text{SiO}_2}(E_{\text{Si}})$.

The ratio R_0 of bulk intensities

Values of R_0 may be determined experimentally or theoretically. It is generally thought to be easier to calculate R_0 from theory because, in conducting measurements for the experimental approach, the absolute intensity stability of the instrument must be maintained, any changes in surface roughness controlled and any contamination effects minimized. These issues cause unwanted uncertainties. Many instruments cannot achieve the required absolute intensity stability from sample to sample because of the sensitivity of the instrument's absolute intensity scale to sample position and drift of the x-ray source efficiency. To make an experimental determination of R_0 , the absolute intensity level needs to be maintained on changing from the samples of pure Si to those of pure SiO₂. Furthermore, both materials will be contaminated with carbonaceous and water layers on entry to the spectrometer, and these will affect the absolute intensities measured. Unfortunately, the contamination cannot be removed without sputtering. Sputtering, unfortunately, can alter the surface zone by implanting $\sim 5\%$ argon and can significantly reduce the oxygen level by preferential sputtering. These issues lead to uncertainty in the experimental measurement of R_0 . For these reasons, some analysts have preferred to calculate R_0 . Later we shall address the above measurement issues.

Calculation of the absolute value of R_0 is relatively straightforward for successive measurements in the same instrument using the same experimental conditions. Thus

$$R_0 = \frac{N_{\text{SiO}_2} Q_{\text{SiO}_2}(E_{\text{Si}}) \lambda_{\text{SiO}_2}(E_{\text{Si}})}{N_{\text{Si}} Q_{\text{Si}}(E_{\text{Si}}) \lambda_{\text{Si}}(E_{\text{Si}})} \quad (3)$$

where the N values are the atomic densities of the silicon atoms in SiO₂ and Si, respectively, the Q values are as defined by Jablonski's² analysis of the effects of elastic scattering and the λ values are the inelastic mean free paths (IMFPs) for electrons from silicon at energy E_{Si} in SiO₂ and Si, respectively. The atomic number densities may be obtained from the respective bulk densities ρ_{SiO_2} and ρ_{Si} and the atomic or molecular masses M_{SiO_2} and M_{Si} . Thus

$$R_0 = \frac{\rho_{\text{SiO}_2} Q_{\text{SiO}_2}(E_{\text{Si}}) \lambda_{\text{SiO}_2}(E_{\text{Si}}) M_{\text{Si}}}{\rho_{\text{Si}} Q_{\text{Si}}(E_{\text{Si}}) \lambda_{\text{Si}}(E_{\text{Si}}) M_{\text{SiO}_2}} \quad (4)$$

Values of ρ_{Si} , M_{Si} and M_{SiO_2} are known accurately as 2.32908 g cc⁻¹, 28.0855 and 60.0843, respectively.³ Values for ρ_{SiO_2} , however, are not as well known. For α -quartz, the values of 2.650 and 2.648 g cc⁻¹ are given,^{3,4} with lower values for other crystalline forms and 2.196 g cc⁻¹ for vitreous or amorphous quartz.⁴ This latter value seems to be the form generally thought to be closest to the thermal oxide formed on silicon. Values of the IMFP have been calculated by Tanuma *et al.*^{5,6} and are given in Table 1 for the relevant photoelectron energies for Mg and Al x-rays. The values of Q are only available for certain levels and elemental solids in Jablonski's tables² and so here we make use of fits to those data based on transport theory. For elements with $\omega \leq 0.245$, Q is given by⁷

$$Q = (1 - \omega)^{0.5} (1 + 0.412\omega) \quad (5)$$

where ω is the ratio $\lambda/(\lambda + \lambda_{tr})$ and λ_{tr} is the transport mean free path. The value of ω may be determined from Jablonski and Powell's table 1 data⁸ or from the plots derived from these data by Seah and Gilmore.⁷ For compounds we then use⁷

$$\omega_{cpd} = \sum_k X_k \omega_k \quad (6)$$

where X_k is the atomic fraction of the k th constituent of the compound. The Q values so calculated are also given in Table 1.

Using $\rho_{SiO_2} = 2.196 \text{ g cc}^{-1}$ we find

$$R_o(\text{Mg}) = 0.530 \quad (7)$$

$$R_o(\text{Al}) = 0.529 \quad (8)$$

The accuracy of these values depends on the accuracy of the value of ρ_{SiO_2} and the accuracies of the IMFP values used in Eqns (3) and (4). Powell and Jablonski⁹ have carefully analysed recent sets of experimental data for measurements of the IMFPs for Si at different energies. In that review, the fits to the four elastic peak reflection data sets given for λ_{Si} in the kinetic energy range 800–2000 eV may be evaluated to show that the ratio of theoretical and experimental values is 0.82 ± 0.09 , indicating a significant possible error in the predictions for the IMFP of Si. Equivalent measurements for the IMFPs in SiO_2 do not exist but we may estimate values from the measured attenuation lengths L_{SiO_2} .

Calculations of the value of L , which is valid for layers thicker than one monolayer but thinner than $3\lambda \cos \theta$ and for angles of emission $\leq 58^\circ$ from the surface normal, have been made by Cumpson and Seah.¹⁰ These calculations are for the same 27 elements for which IMFP values (λ) were calculated by Tanuma *et al.*⁵ In terms of the ratio L/λ for Si, it is found that⁷

$$L/\lambda = 0.979[1 - \omega(0.955 - 0.0777 \ln Z)] \quad (9)$$

This equation is valid with a scatter of 1.2%⁷ about the Monte-Carlo calculations.¹⁰ and may be used directly for Si with $Z = 14$ but for compounds we need the average value of Z (10 for SiO_2) and we need to deduce the relevant value of ω from Eqn (6).

Values of L/λ for Si and SiO_2 are given in Table 1. Typical values range from 0.885 to 0.918 for electrons in SiO_2 . Recent analyses by Powell and Jablonski using the

transport approximation give L/λ values 0.9% higher¹¹ for these conditions. In this way, we may compare the theoretical and measured L values for Si and SiO_2 from the experimental compilations of L , for overlayer experiments using Mg and Al x-rays, by Powell and Jablonski.⁹ Thus, we find that the ratios of the theoretical and experimental L values are 1.06 ± 0.26 and 1.08 ± 0.18 for Si and SiO_2 , respectively. At a level of 10%, experiment and theory agree. The overlayer experiments give values for L that are slightly lower than those of the theoretical calculations, whereas the elastic peak reflection data for Si, described earlier, give experimental values of λ that are somewhat higher than theory.

From the discussions above, calculations for both x-ray sources give

$$R_o(\text{Mg, Al}) = 0.53 \pm 0.05 \quad (\text{theory}) \quad (10)$$

based on Eqn (3) or (4) and the uncertainties in the IMFP values.^{5,6} Similar values of R_o have been calculated by Ebel *et al.*¹² and by Gross *et al.*,¹³ the latter using $\rho_{SiO_2} = 2.22 \pm 0.03 \text{ g cc}^{-1}$. Experimental data for R_o have been compiled in many studies, as shown in Table 2. The average and standard deviation values for these are given by

$$R_o(\text{Mg, Al}) = 0.76 \pm 0.08 \quad (\text{experiment}) \quad (11)$$

Clearly, experiment and theory differ significantly. If Eqns (3) and (4) are valid, this discrepancy would need ρ_{SiO_2} or λ_{SiO_2} individually to be increased by at least a factor of 1.30, or both to be increased by factors of 1.14. Although many of the experimental data are for samples exhibiting carbonaceous contaminations, which will be at different levels for the Si and SiO_2 reference samples, the contamination in general will, only cause a small attenuation of the intensities and among the 10 separate data sets in Table 2 may well be random. The experimental data are therefore probably not very biased. We may obtain a theoretical value of R_o closer to the experimental value by assuming that the thermal oxide has the bulk density of α -quartz (2.648 g cc^{-1}) and by retaining the same calculated value of λ_{SiO_2} as before.⁶ In this case, the theoretical value of $R_o(\text{Mg, Al})$ rises to 0.64 ± 0.06 . However, the density of 2.196 g cc^{-1} used earlier for SiO_2 is close to: the value of 2.19 g cc^{-1} used by Tanuma *et al.*⁶ in their calculations of λ ; the deduced values of 2.07 – 2.25 g cc^{-1} from optical data for native oxides on Si;²³ the deduced value of 2.21 g cc^{-1} for thermal oxides by neutron reflectometry;²⁴

Table 1. Summary of numerical data for Mg and Al x-rays

X-rays	Mg					Al				
	SiO ₂		Si	C (glassy)	C (polymer)	SiO ₂		Si	C (glassy)	C (polymer)
Material	Si 2p	O 1s	Si 2p	C 1s	C 1s	Si 2p	O 1s	Si 2p	C 1s	C 1s
Electrons	Si 2p	O 1s	Si 2p	C 1s	C 1s	Si 2p	O 1s	Si 2p	C 1s	C 1s
Energy (eV)	1150	722	1150	970	970	1383	955	1383	1203	1203
IMFP (nm)	3.264	2.291	2.729	2.645	2.994	3.756	2.834	3.147	3.119	3.547
Q	0.988	0.983	0.983	0.990	0.990	0.991	0.987	0.986	0.992	0.992
L/λ	0.908	0.885	0.885	0.913	0.913	0.918	0.900	0.897	0.923	0.923
L (nm)	2.964	2.028	2.415	2.415	2.734	3.448	2.551	2.823	2.879	3.274

Table 2. Experimental values of R_o , in chronological order

Authors	Ref.	R_o	X-rays	Comment
Hill <i>et al.</i>	14	0.672 ± 0.050	Al	Bulk samples, contaminated
Ishizaki <i>et al.</i>	15	0.779 ± 0.019	Mg	Deduce from Eqn (3), using thermal oxide
Hochella and Carim	16	0.82 ± 0.01	Al, Mg	Lightly sputtered Si and thermal oxide
Fulghum <i>et al.</i>	17	0.94	Al, Mg	Deduced by fitting a rearranged version of Eqn (2)
Fulghum	18	0.71	Al, Mg	Deduced from their fig. 6 data
Mitchell <i>et al.</i>	19	0.75 ± 0.02	Al	Xe sputtered and corrected for Xe implantation
Mitchell <i>et al.</i>	19	0.70 ± 0.01	Al	Deduce from Eqn (3), samples have low contamination
Yano <i>et al.</i>	20	0.67	Mg	Clean Si and thermal oxide
Lu <i>et al.</i>	21	0.75	Al	H-terminated Si and thermal oxide
Cole <i>et al.</i>	22	0.833	Al	HF-etched Si and thermal oxide
Mean \pm SD		0.76 ± 0.08	Al, Mg	

the deduced value of 2.24 g cc^{-1} from x-ray reflectometry.²⁴ From the literature, therefore, we view 2.196 g cc^{-1} as the best estimate for the thermal oxide density and 0.53 ± 0.05 as the best available theoretical estimate for R_o .

The SiO₂ attenuation length

So far, in applying Eqn (2) to deduce d_{oxide} we need both R_o and L_{SiO_2} . The value of R_o , as we have seen, may be calculated or measured experimentally and, at present, there is a significant difference. If we have samples with known values of d_{oxide} , we may use Eqn (2) to deduce experimental values of L_{SiO_2} to compare with the theoretical calculations if we have a value for R_o . Uncertainties in R_o lead to uncertainties in the derived value for L_{SiO_2} , as discussed by Fulghum.¹⁸ For an oxide thickness of 3 nm, the difference between the R_o values of Eqns (10) and (11) leads to a difference in the deduced L_{SiO_2} values of 18%, with L_{SiO_2} increasing roughly as $R_o^{0.5}$.

It is useful to consider the correlation of L_{SiO_2} and R_o in calibrations using Eqn (2) with a range of samples where a calibration is either done, or is best, at one thickness, i.e. the uncertainties are lowest at this thickness. This will illustrate certain points. For this illustration, given in Fig. 2, we assume that samples exist in the range 0.5–10 nm but that the sample with 4 nm of oxide has no uncertainty (i.e. is the best calibration point) and we have calculated what the intensity ratios should be for a range of 'true'

thicknesses, shown on the abscissa for $L_{\text{SiO}_2}(\text{Mg}) = 2.964 \text{ nm}$ and $R_o = 0.76$. We now use these intensity ratios as if they were measured and, using R_o values between 0.5 and 1.0, calculate the oxide thicknesses that we would deduce for each R_o value, as shown in Fig. 2(a). The ratio of these deduced thicknesses to the true thicknesses is then shown in Fig. 2(b). What these curves show is that, for the single-point calibration at 4 nm, an uncertainty of ± 0.05 (i.e. 7%) in R_o can appear to be offset by an uncertainty of $\pm 0.1 \text{ nm}$ (i.e. 3.5%) in $L_{\text{SiO}_2}(\text{Mg})$. More importantly, an offset in all of the original calibration thicknesses arising from a bias or offset in the method for determining d_{oxide} (e.g. the use of nuclear reaction analysis, NRA, to determine the number of oxygen atoms m^{-2} where a monolayer of water adds oxygen signal equivalently for all thicknesses, or the use of ellipsometry where the carbonaceous and water layers add to all of the measured thicknesses) would lead to an excellent calibration line requiring an artificially reduced value of R_o . If the offset is 0.34 nm, an apparent drop in the value of R_o to 0.5 and an apparent reduction in L by 7% would fit film thicknesses in the range 0–10 nm. Thus, small systematic errors in the oxide thicknesses may lead to significant errors in the R_o values deduced from fitting data to Eqn (2); however, the corresponding errors in L_{SiO_2} are relatively weaker. It is thus important to consider independent measurements of L_{SiO_2} and R_o . Let us now consider the attenuation lengths (ALs) more carefully to try to define the absolute values.

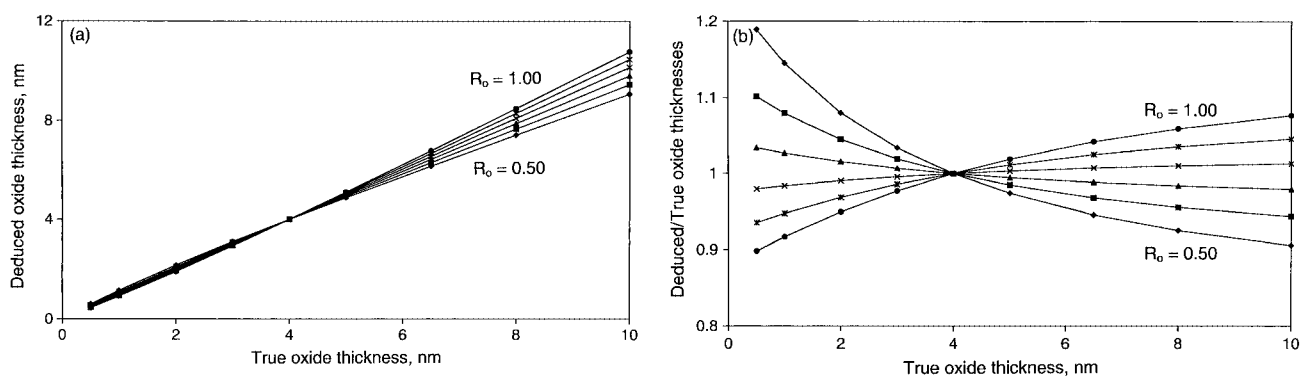


Figure 2. Deduced thicknesses (a), and the ratio of the deduced and true thicknesses (b), using Eqn (2) for various values of L_{SiO_2} (Mg) and for R_o values of 0.5–1.0 in steps of 0.1, assuming a single-point calibration at 4 nm. For the sake of illustration, it is assumed that $L_{\text{SiO}_2}(\text{Mg}) = 2.964 \text{ nm}$ and $R_o = 0.76$ are the correct values.

Using the approach of Seah and Gilmore⁷ with Cumpson and Seah's¹⁰ calculations, which in turn depend on the calculations of Tanuma *et al.*,^{5,6} we obtain the theoretical values for L/λ given in Table 1 and hence

$$L_{\text{SiO}_2}(\text{Mg}) = 2.964 \text{ nm (theory)} \quad (12)$$

$$L_{\text{SiO}_2}(\text{Al}) = 3.448 \text{ nm (theory)} \quad (13)$$

These L values are valid for oxides up to ~ 9 nm thick and for angles of emission $\leq 58^\circ$ from the surface normal. The recent detailed calculations of Powell and Jablonski¹¹ for a similar thickness and angle of emission range up to 55° give

$$L_{\text{SiO}_2}(\text{Mg}) = 2.905\text{--}3.036 \text{ nm (theory)} \quad (14)$$

$$L_{\text{SiO}_2}(\text{Al}) = 3.392\text{--}3.546 \text{ nm (theory)} \quad (15)$$

The centre values of these ranges agree with the Seah and Gilmore values to a level much better than 1%. The closeness of these values arises from the good accuracy of the elastic scattering analyses^{7,10,11} but both approaches depend on the same original calculation of IMFP by Tanuma *et al.*^{5,6} for which an average uncertainty of 10% is cited.⁵

As noted earlier, the correlation of theory and experiment for L_{SiO_2} , as listed by Powell and Jablonski,⁹ gives a value for the ratio of theory to experiment of 1.08 ± 0.18 . Published results using the overlayer method are given in Table 3. These give

$$L_{\text{SiO}_2}(\text{Mg}) = 2.85 \pm 0.46 \text{ nm (experiment)} \quad (16)$$

$$L_{\text{SiO}_2}(\text{Al}) = 3.14 \pm 0.31 \text{ nm (experiment)} \quad (17)$$

These average experimental values are ~ 0.939 of the theoretical values. If the original published data in Table 3

are adjusted, where relevant, for $R_0 = 0.76$, this average rises to 0.970 of the average theoretical values. This consistency is excellent.

Effects of crystallinity

In two of the studies mentioned so far, effects of crystallinity have been observed, modifying $I_{\text{Si}_{\text{met}}}$. Hill *et al.*¹⁴ observe structure in the intensities as a function of θ of the order of $\pm 16\%$ for thinner oxides. This effect reduces as the oxide thickness increases. Mitchell *et al.*,¹⁹ on the other hand, make measurements at fixed angles of emission θ and vary the azimuthal angle ϕ . They find intensity changes of $\pm 6\%$, with sharp minima associated with the orientations of rows of Si atoms of the substrate. These intensity variations, even if R_0 and L_{SiO_2} are accurately established, may limit the precision of oxide thickness determination by XPS using Eqn (2). Information on the geometrical conditions of the published experimental data are summarized in Table 3.

Effects of carbonaceous contamination

Determination of the oxide thickness from Eqns (1) and (2) should not be affected by contamination because the Si 2p intensities from both the metal and the oxide peaks are equally attenuated. However, in measuring R_0 , contamination is important because the contamination levels may be different on the bulk Si and the bulk SiO_2 . We therefore establish the equations here, for the measured intensities, for use later. These intensities are given by

$$I_{\text{Si}_{\text{met}}} = I_{\text{Si}_{\text{met}}}^{\infty} \exp[-d_C/L_C(E_{\text{Si}}) \cos \theta] \quad (18)$$

$$I_{\text{SiO}_2} = I_{\text{SiO}_2}^{\infty} \exp[-d_C/L_C(E_{\text{Si}}) \cos \theta] \quad (19)$$

Table 3. Experimental values of L_{SiO_2} using Si 2p electrons, in chronological order

Authors	Ref.	Si surface	Angle of emission ^a	L_{SiO_2} (Mg) (nm)	L_{SiO_2} (Al) (nm)	Traceability
Hill <i>et al.</i>	14	(100)	Averaged		3.7 ± 0.4	Ellipsometry
Ishizaki <i>et al.</i>	15	(100)	42.5° ^b	3.49 ± 0.01		Ellipsometry
Ebel and Liebl	25	—	Averaged	3.083	3.160	Ellipsometry
Hochella and Carim	16	(100)	0°	2.13 ± 0.06	2.57 ± 0.06	TEM
Ebel <i>et al.</i>	12	—	Averaged	2.71	3.20	Ellipsometry
Fulghum <i>et al.</i>	17	(100)	45°	3.0	3.5	Ellipsometry, RBS
Fulghum	18	(100)	Averaged		3.19 ± 0.20	Ellipsometry, RBS
Mitchell <i>et al.</i>	19	(100)	15°		2.93 ± 0.06	NRA
Yano <i>et al.</i>	20	(111)	0°	2.7		TEM
Lu <i>et al.</i>	21	(100)	12.5°		3.04 ± 0.11	TEM
					($d > 4$ nm)	
Gross <i>et al.</i>	13	(100)	0°		3.03 ± 0.14 ^c	Ellipsometry
	13	(100)	15°		2.82 ± 0.15 ^d	Ellipsometry
Cole <i>et al.</i>	22	(100)	25°		3.351 ± 0.044 ^e	TEM, RBS
Mean \pm SD				2.85 ± 0.46	3.14 ± 0.31	Various

^a No azimuths are given for any of the data; 'averaged' indicates that the data were taken over many emission angles and the value of the attenuation length was deduced from a fitting of Eqn (2) to a range of angles.

^b Data recorded using a cylindrical mirror analyser so that all azimuths are averaged.

^c Deduced from supplementary data for Ref. 13, provided by W. Unger for an average of Si 2p and 2s data.

^d Deduced from supplementary data for Ref. 13, provided by W. Unger for Si 2s data.

^e Deduced from supplementary data for Ref. 22, provided by D. A. Cole.

There are other important effects of the contamination and these are dealt with in Part I.¹

EXPERIMENTAL

In this work, most of the analysis is conducted from material of one set of polished Si(100) wafers cut into squares bounded by the (111) planes, defining [110] directions such that the azimuthal zero of the angle is along the [110] direction. Angles of emission are defined from the sample surface normal. Some work was also conducted on other (100) material and also (111) wafers cut into triangles also bounded by (111) planes that define [110] directions.

All XPS analyses in this work were conducted in a VG Escalab II spectrometer with a five channel electron multiplier detector using either 20 or 50 eV pass energy and 6 mm input and output slits. Except where stated otherwise, Mg x-rays were used for the (100) surfaces and the angle of emission was set at 27° or 28.5° from the surface normal in the [110] azimuth. In all of the work, the x-ray angle of incidence was set so that the average angle between the incident x-ray direction and the electron angle of emission was 54.7° (i.e. the magic angle). The instrument intensity/energy response function²⁶ was determined prior to recording the data.

As a result of different cleaning procedures detailed elsewhere,¹ the surface may be covered by carbonaceous overlayers only 0.12 nm thick, or deliberately of varying thickness in a range up to a few nanometres by adding contamination. Unless stated otherwise, the samples are cleaned by a 16 h soak in isopropyl alcohol (IPA), followed by a 1 min ultrasonic clean in fresh IPA with the solvent removed by a jet of argon gas. A typical widescan spectrum in this state is shown in Fig. 3(a) and details of the Si 2p peaks in Fig. 3(b). Here, we measure the total C 1s intensity, I_C , the total O 1s intensity, I_O , the total Si 2p intensity, $I_{\text{Si tot}}$, and the silicon intensities for the metal and oxide, $I_{\text{Si met}}$ and I_{SiO_2} . In all cases, to measure intensities, the x-ray satellites are removed,

followed by a general Shirley²⁷ background. In the case of the separate components of the silicon metallic and oxide states, the Si 2p peak is further reduced by removal of the spin-orbit splitting, by deconvolving with a structure comprising 50% intensity at 0.6 eV higher binding energy²⁸ before Shirley background removal. The structure that remains is shown in Fig. 3(b). This is then separated into its five constituent peaks using Gaussian/Lorentzian sum function peaks. We separate the SiO₂, Si₂O₃, SiO and Si₂O peaks as having binding energies higher than that for Si (by 3.8–4.3, 2.48, 1.75 and 0.95 eV, respectively), as defined by Himpsel *et al.*²⁹ and by Keister *et al.*³⁰ The total oxide thickness is then calculated as noted earlier.

Towards the end of the experiments, sputter removal of both the oxide and the carbonaceous contamination is made by sputtering using an argon ion gun mounted 45° to the surface normal and delivering 5 keV ions at current densities of either 1 or 10 $\mu\text{A cm}^{-2}$. This sputtering is conducted with sample rotation in a preparation chamber with ultrahigh vacuum base pressure.

RESULTS AND DISCUSSION

Effect of contamination on the oxide thickness deduced from Eqn (2)

We may deduce a thickness for the oxide simply from Eqn (2) by using Eqn (12) for $L_{\text{SiO}_2}(\text{Mg})$ and either Eqn (10) or Eqn (11) for R_o . This gives us two possible thicknesses, depending on the validity of the theoretical or experimental values of R_o . We may plot these values as a function of the carbon contamination level, which is calculated here for an average polymer.¹ If we were to calculate for the contamination being glassy, rather than an average polymer, the abscissa values should be reduced by a factor of 2.59.¹ If the contamination is expressed in carbon atoms m^{-2} , 1 nm of the glassy carbon or 2.59 nm of the average polymer are equivalent to 1.148×10^{20} carbon atoms m^{-2} . In that expression of the amount of contaminant, the form becomes

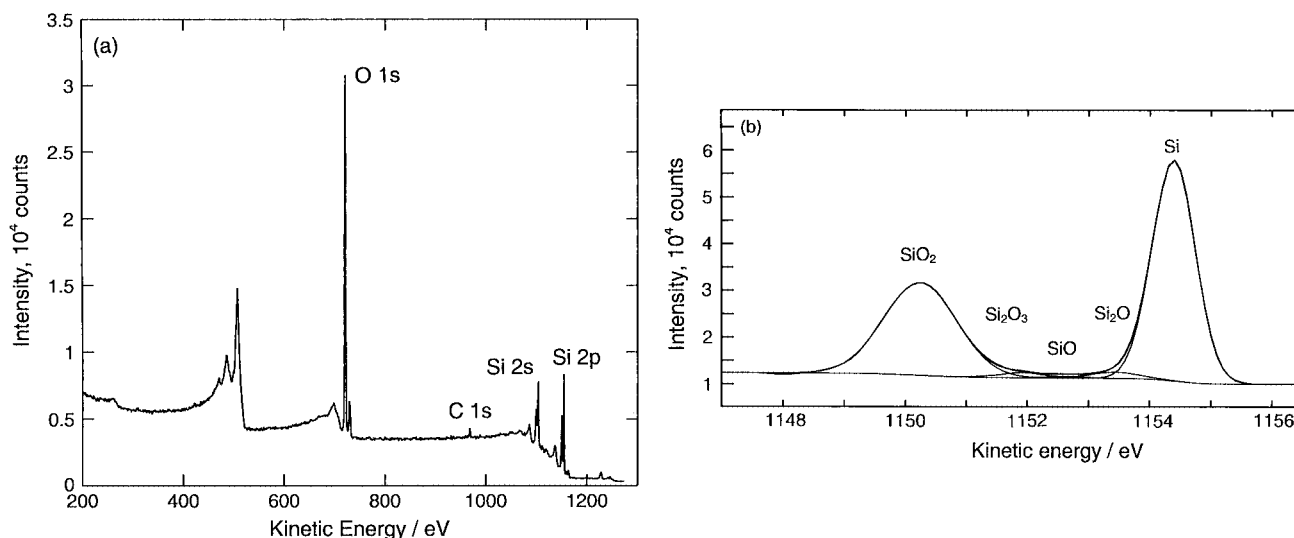


Figure 3. The XPS data for a sample with ~2 nm of oxide, cleaned as described in the text, using Mg x-rays and the geometry of position 'A' with an analyser resolution of 0.4 eV: (a) widescan; (b) the Si 2p peaks after satellite and spin-orbit splitting removal, showing the Shirley background and the peak synthesis.

irrelevant.¹ We still show thicknesses in nanometres for an average polymer in the diagrams, because analysts are used to these thicknesses and can easily judge the general cleanliness of the surface.

Figure 4 shows the calculated oxide thicknesses for samples from one wafer with different levels of contamination for the two values of R_0 . The results show a small apparent increase in the oxide thickness as the contaminant level rises. This is $\sim 1.4\%$ of the oxide thickness for an additional average polymer carbonaceous contamination thickness equivalent to the full oxide thickness. This very small increase may occur as a result of the increase in background following the peak as the carbon level rises, coupled with the shortcomings of the Shirley background method. However, if we project from the data for the relatively clean surfaces, which may be generated routinely,¹ to those of surfaces with no contamination at all, the thickness is reduced by <0.003 nm. This is significantly below the uncertainty of the measurements and thus, in general, the small increase may be ignored.

Effect of crystal orientation

One piece of material was mounted on the sample holder with the azimuthal rotation angle set at 0° . The sample was then tilted from -12° to $+78^\circ$ in 3° steps and the spectrum for the Si 2p peak recorded at each angle. The azimuthal angle was then increased to 22.5° and then to 45° , and the above set of data repeated each time. Figure 5 shows the calculated oxide thickness from each of these experiments using $R_0 = 0.76$. The smoothness of the curves indicates a measurement precision at one standard deviation of 0.003 nm. These data show very similar results to those of Mitchell *et al.*¹⁹ Maxima of the crystalline substrate intensities occur along the crystallographic directions indicated on the curves. These maxima are associated with elastic scattering and interference with strong forward focusing^{31,32} along the low index rows and, for instance, at the [100] pole represents an intensity increase of 30% compared with the regions 10° away from the pole. The intensities of the carbonaceous contamination and of the silicon oxide, however, do not vary significantly across this pole. These effects lead to thickness minima with a full width at half-maximum (FWHM) of

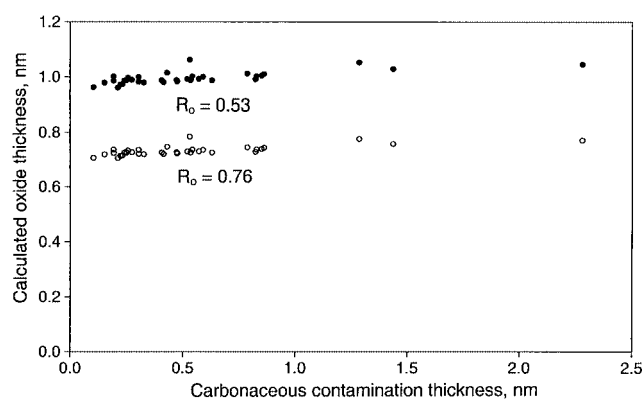


Figure 4. Effect of contamination on the oxide thickness calculated from Eqn (2): (●) using the theoretical value of $R_0 = 0.53$ from Eqn (10); (○) using the experimental value of $R_0 = 0.76$ from Eqn (11).

9° , compared with 17° in Mitchell *et al.*'s work where the spectrometer had a 15° acceptance angle. In the present work, the internal electron optics of the spectrometer limits the range of angles in the tilting direction to 7.5° and in the orthogonal direction to 12° (these are the total angles that could otherwise be written $\pm 3.75^\circ$ and $\pm 6^\circ$, respectively). Note that there is a strong peak in intensity at 0° . This will lead to a low effective value of R_0 being required for Eqn (2) for determining the oxide thickness for 0° emission. If an average value of R_0 is used, an erroneously high value of L_{SiO_2} may be deduced at this geometry.

Results in the literature³² show that, with appropriate equipment, diffraction features with FWHM at 4° are observed. To evaluate the sensitivity of the data to the angular resolution of the instrument, we have analysed the region shown in Fig. 5(a) around the [100] pole. To do this, we have simply set all of the lens voltages to ground. The intensities are reduced but are still adequate for measuring the Si 2p intensities of the elemental and oxide states. Figure 6 shows the resulting deduced oxide thicknesses based on these measurements interpreted in the same manner as in Fig. 5. With this configuration, the spectrometer accepts electrons over an angular range of only 0.7° and, as can be seen in Fig. 6, the data have structure with this level of detail. Unfortunately, our sample tilt mechanism has only this level of resolution and so the major uncertainty is in the abscissa and not the ordinate. The curve shown in Fig. 6 is drawn through the average results for the data at positive and negative emission angles so that the symmetry of the data is clear.

In Fig. 7, the results measured with the spectrometer input lens activated are marked on the stereographic triangle with circles at the major poles, approximately reflecting the FWHM of the thickness minima. It is clear that the crystallographic influence on the Si substrate intensity can make the use of Eqn (2) somewhat imprecise. Figure 5(a) shows that our original choice of 27° in the [011] azimuth, position B, sits nicely between the two minima for the [411] and [211] directions that occur at 19.5° and 35° to the surface normal. Between the 21° and 39° angles of emission the deduced oxide thickness only changes over a range of $\pm 3\%$. Although this is good, we can reduce the uncertainty further by working well away from a low-index crystal direction. Figure 5(b) shows results for an azimuth containing high-index directions. We see a flattish region in the range $24\text{--}39^\circ$ emission angle, where the deduced thickness increases by $<6\%$. Near the middle of this range (at 34° emission angle, position A), a change of 1% occurs for a 3° change in angle. A precision of setting the crystal geometry to better than 3° should be achieved fairly readily in all spectrometers and so we define orientation 'A' in Fig. 7, at an angle of emission of 34° , to be at 22.5° in between the [011] and [001] azimuths and 'B' at an angle of emission of $27\text{--}28.5^\circ$ in the [110] azimuth, as reference orientations. These orientations are relatively insensitive to the precise geometry of the sample and are suitable for spectrometers with an acceptance cone full angle of up to 18° and, for 'A', probably up to 40° .

Although in much of the rest of this paper we shall use orientation 'B', it is orientation 'A' that is recommended for

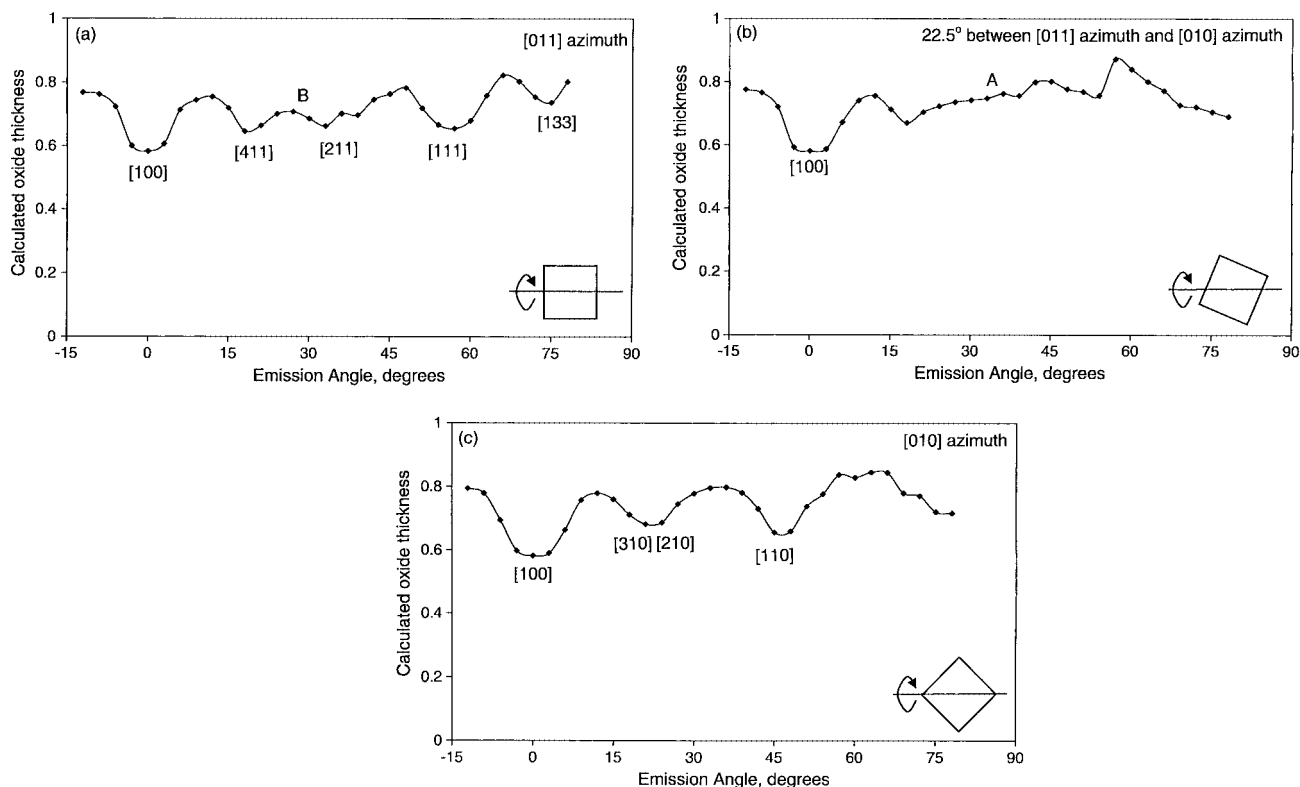


Figure 5. Calculated oxide thicknesses for the (100) surface from Eqn (2) using $R_o = 0.76$ for changes in the angle of emission θ for: (a) $\phi = 0^\circ$, [011] azimuth; (b) $\phi = 22.5^\circ$; (c) $\phi = 45^\circ$, [010] azimuth. The crystal directions are noted on the plots. The small symbol in the lower right of each plot shows the rotation in relation to the wafer piece.

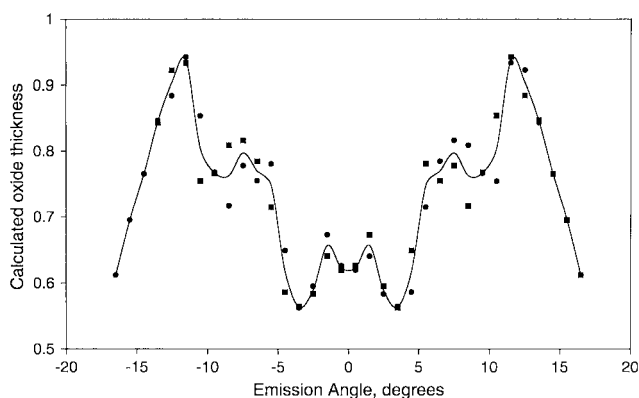


Figure 6. Detail of Fig 5(a) around the [100] pole with the spectrometer lens turned off. The data depicted (●) have been added to the plot as a second value mirrored about the zero emission angle and are shown (■). The smooth curve is drawn through the average where the two data values occur.

future work. The thickness deduced in orientation A is 6.8% higher than at orientation B if we use the same ALs and R_o values. It is not clear to which geometry the deduced ALs of Eqns (12)–(15) are relevant, but it seems reasonable to assume that because the overlayers are amorphous the ALs do not change with orientation but the value of R_o will be changed. We therefore assume that both relate to an average geometry and that this may be realised by an average over the data in Fig. 5. We do not simply average all of the data because the validity of Eqns (12)–(15) degrades rapidly for angles of emission greater than 65° .^{10,11} Additionally,

the [100] pole direction is counted in all three data sets. Using the data from 10° to 65° from each data set once, together with the value around the [100] pole and $R_o = 0.76$, gives an average calculated oxide thickness of 0.733 ± 0.064 nm, with most of the scatter arising from the few data points at the low-index directions. The result at orientation 'B' is 0.958 of this average and that at orientation 'A' is 1.023 of this average. This confirms the use of orientation 'A' as a good reference position.

Detailed intensity measurements for a (100) surface have been made by Han *et al.*³³ in their work on Cu. Their results at 5° increments in azimuth show how the intensity maxima around the low-index poles vary as described here but that, in addition, the maxima at the [411] and [211] poles are streaked azimuthally.

Experiments were now conducted with (111) material that had a slightly different oxide thickness from the (100) material used so far. In this case, the [111] pole is normal to the surface and this has a significant forward-focusing effect, as seen by the minima in Figs 5(a) and 8(a). Unfortunately, the region of the [111] pole is not symmetrical if we tilt with positive angles of emission from [111] to [011], as in the reverse direction where we move to [100]. Figure 8(a) shows these results with the pole directions marked. There are two sets of measurements marked with different symbols. Because we can only tilt from -12° to 80° , one set of measurements is recorded after the other by rotating the sample azimuthally through 180° . In this plot we can clearly see the structure of Fig. 5(a) and so we note here the position B. By rotating the azimuth of the wafer piece by 30° we

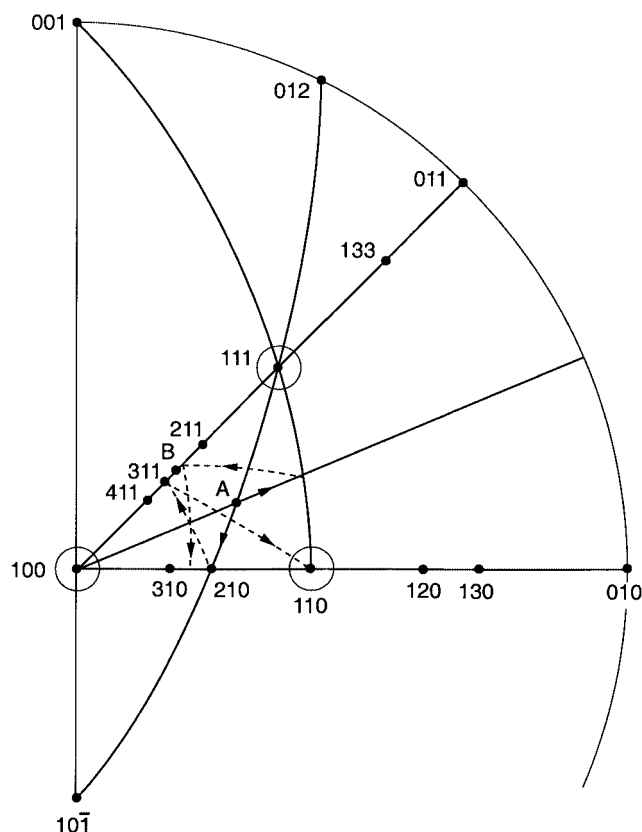


Figure 7. Polar plot showing the thickness minima in Fig 5 at the major poles. Other minima (shown in Figs 5 and 8) occur but are omitted for clarity. The data in Figs 5 and 8 follow lines or great circles in the polar plot, which, by symmetry, fold back on themselves as shown by the dashed lines in the stereographic triangle.

may tilt in the plane containing the $[10\bar{1}]$ and $[\bar{1}01]$ azimuths, which pass through our earlier point A. Note how point A, accessible for both (100) and (111) surfaces, is again far from a maximum in the $I_{\text{Si}}^{\text{met}}$ intensity and hence from a minimum in the deduced thickness. We thus recommend point A at 34° from the $[100]$ pole in the azimuth to be at 22.5° in between the $[011]$ and $[001]$ azimuths, or at 25.5° from the $[111]$ pole in the $[10\bar{1}]$ azimuth, for the (100) and (111) surfaces, respectively. These angles, it should be noted, assume that the surfaces

are polished exactly in the correct orientation. This is not always the case, and the data for Figs 8(a) and 8(b) have been calculated by assuming 2° and 2.5° angular offsets, respectively, so that the $[111]$ pole appears at 2° and 2.5° in each of these figures. Again, Han *et al.*³³ give detailed results for the (111) surface of Cu that agree with the present data but are more detailed and show the azimuthal streaking.

Effect of carbonaceous contamination on the silicon intensities

In Part I¹ we analysed the effects of the carbonaceous contamination in order to determine the effectiveness of cleaning methods. Extra data from that work allow us to evaluate the effect of carbon on the silicon signals.

The carbon intensity, I_C , is given by

$$I_C = I_C^\infty \{1 - \exp[-d_C/L_C(E_C) \cos \theta]\} \quad (20)$$

where I_C^∞ is the intensity for bulk carbonaceous contamination, d_C is the thickness of the contamination layer and $L_C(E_C)$ is the attenuation length of the carbon photoelectrons of energy E_C in the contamination layer. The intensity of the silicon substrate, $I_{\text{Si}}^{\text{met}}$, is

$$I_{\text{Si}}^{\text{met}} = I_{\text{Si}}^\infty \exp[-d_{\text{oxide}}/L_{\text{SiO}_2}(E_{\text{Si}}) \cos \theta] \exp[-d_C/L_C(E_{\text{Si}}) \cos \theta] \quad (21)$$

For the main (100) material used in this study, we have already measured d_{oxide} for position B with 28.5° emission in the $[011]$ azimuth. For $R_o = 0.53$, d_{SiO_2} is 0.949 nm, whereas for $R_o = 0.76$ the value is 0.696 nm. Thus

$$I_{\text{Si}}^{\text{met}} = BI_{\text{Si}}^\infty \exp[-d_C/L_C(E_{\text{Si}}) \cos \theta] \quad (22)$$

where B is 0.695 for $R_o = 0.53$ and 0.766 for $R_o = 0.76$.

Because for both glassy carbon and for an average polymer¹ in the energy range E_C to E_{Si} (970–1150 eV)

$$\lambda \propto E^{0.776} \quad (23)$$

and, because L/λ changes little over this energy range, we may write

$$\frac{I_C}{I_C^\infty} = 1 - \left(\frac{I_{\text{Si}}^{\text{met}}}{BI_{\text{Si}}^\infty} \right)^{1.141} \quad (24)$$

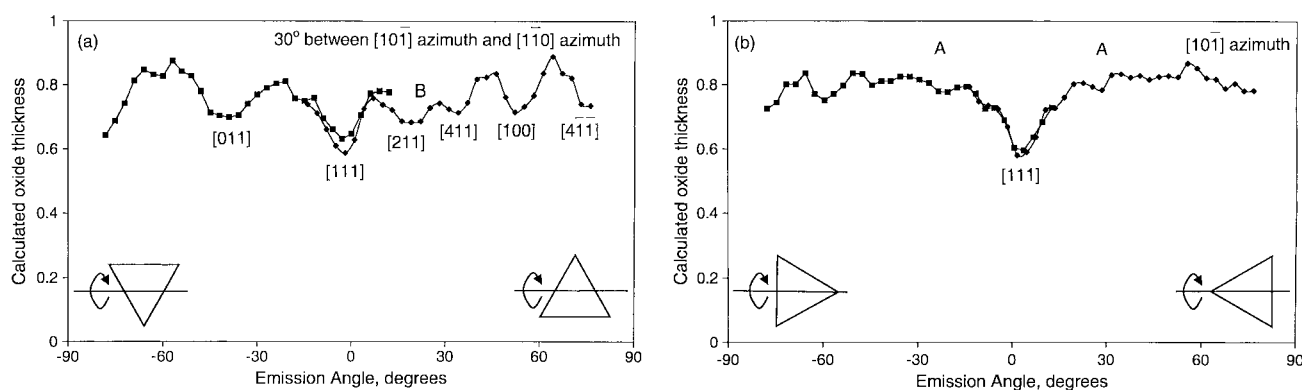


Figure 8. Calculated oxide thicknesses for the (111) surface from Eqn (2) using $R_o = 0.76$ for changes in the angle of emission θ for: (a) the azimuths including the $[100]$ pole; (b) the $[10\bar{1}]$ and $[\bar{1}01]$ azimuths. The small symbols in the lower part of each plot shows the rotation in relation to the wafer piece.

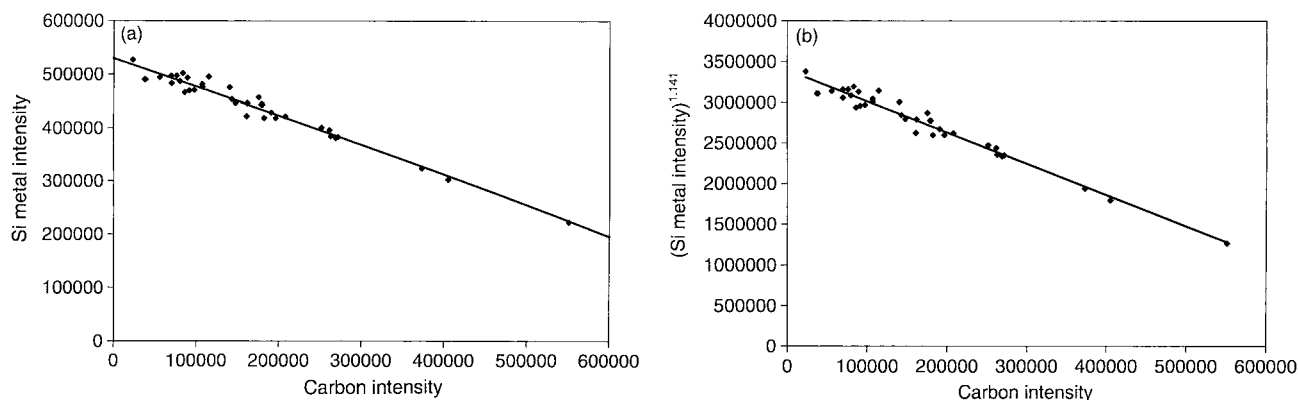


Figure 9. The relationship of the C 1s and Si 2p metallic component-measured intensities (counts \cdot eV s^{-1}) with: (a) ordinate $I_{\text{Si met}}$; (b) ordinate $(I_{\text{Si met}})^{1.141}$. The straight-line fit of (b) is the curve on plot (a). The intensities here are not corrected for the instrument response function.

Figure 9(a) gives a plot of I_C versus $I_{\text{Si met}}$, and Fig. 9(b) a plot of I_C versus $(I_{\text{Si met}})^{1.141}$. From these plots we deduce, before correcting for the instrument intensity/energy response function, that

$$I_C^\infty = 884300 \text{ counts} \cdot \text{eV} \cdot s^{-1} \quad (25)$$

$$I_{\text{Si met}}^\infty = 762557 \quad (R_o = 0.53, \text{ theory}) \quad (26)$$

$$I_{\text{Si met}}^\infty = 691930 \quad (R_o = 0.76, \text{ experiment}) \quad (27)$$

Hence, correcting for the instrument response function

$$\frac{I_C^\infty}{I_{\text{Si met}}^\infty} = 1.082 \quad (R_o = 0.53, \text{ theory}) \quad (28)$$

$$\frac{I_C^\infty}{I_{\text{Si met}}^\infty} = 1.192 \quad (R_o = 0.76, \text{ experiment}) \quad (29)$$

These two different experimental values arise from the two possible corrections for the thin oxide layer.

We may calculate $I_C^\infty / I_{\text{Si met}}^\infty$ in the same way as R_o in Eqns (3) and (4), although we also need other parameters. This is done in Ref. 1 where we finally obtain two values, 2.57 and 1.09, depending on whether the carbonaceous contamination is taken as glassy carbon or as an average polymer, respectively. The results from Eqns (28) and (29) are consistent only with a carbonaceous contamination that has the attributes of an average polymer layer and not of a glassy carbon layer.

These results allow us to provide three conclusions. the quality of the fit in Fig. 9(b) confirms that the sample-to-sample repeatability of the absolute measured Si intensity is $\sim 2.2\%$; we may deduce the elemental Si intensity for a clean sample as 762560 or 691930 counts \cdot eV s^{-1} for $R_o = 0.53$ or $R_o = 0.76$, respectively, without cleaning the sample; and, from the figures above, that the data are consistent if we assume that the contamination is equivalent to an average polymer layer.

Measurements for a second (100) wafer with an oxide layer thickness of 0.724 times that of the earlier film are shown in Fig. 10. From this we deduce $I_{\text{Si met}}^\infty$ values of 722690 and 673500 for $R_o = 0.53$ and $R_o = 0.76$, respectively, consistent with the values given above.

A third method to deduce $I_{\text{Si met}}^\infty$ is to sputter remove the carbonaceous contamination and the oxide *in situ*. The results for this are shown in Fig. 11. The ordinate gives the $I_{\text{Si met}}$ intensity and the abscissa gives the I_{SiO_2} intensity. The start of the profile is to the right, where I_{SiO_2} is high, and the finish is to the left. After the first three data points to the right, most of the carbon signal is removed. We see that the effect of carbon, at this level of cleanness, is negligible. As we move to the left, argon is implanted to a few per cent but it is not clear how much this will depress the intensities. The plot shows data for the first and second wafers mentioned above with calculated oxide thicknesses of 0.733 nm and 0.531 nm,

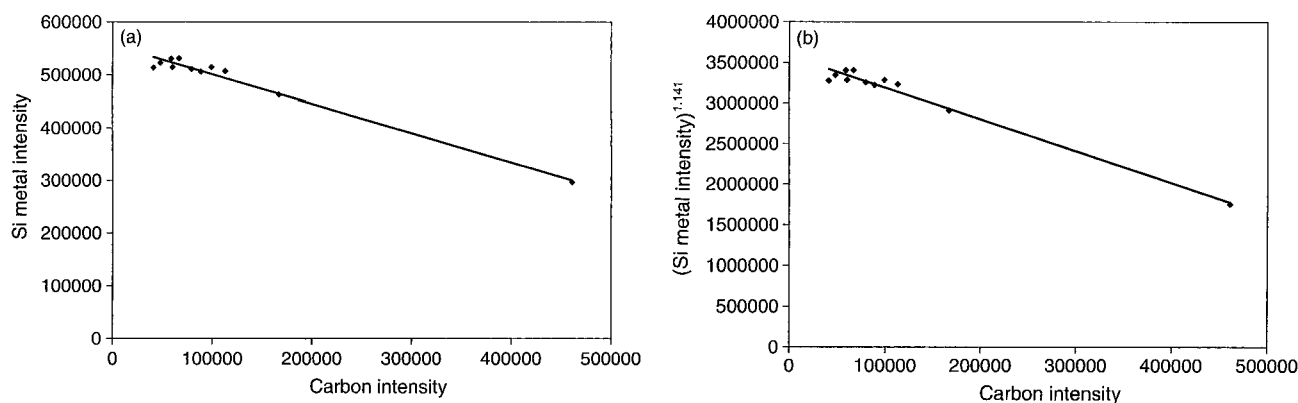


Figure 10. As Fig 9 but for a thinner oxide film.

respectively, based on $R_o = 0.76$. From Eqn (1)

$$I_{\text{Simet}} = I_{\text{SiO}_2}^{\infty} - (I_{\text{SiO}_2})/R_o \quad (30)$$

The straight lines are fits to the data and from the gradients we deduce

$$R_o = I_{\text{SiO}_2}^{\infty}/I_{\text{SiO}_2}^{\infty} = 0.857 \quad (0.696 \text{ nm oxide}) \quad (31)$$

$$R_o = I_{\text{SiO}_2}^{\infty}/I_{\text{SiO}_2}^{\infty} = 0.849 \quad (0.504 \text{ nm oxide}) \quad (32)$$

We cannot use the absolute intensity values for I_{SiO_2} directly from this plot because the higher gas load in sputtering has changed our x-ray source efficiency. Earlier we noted that absolute measurements are not popular, and this is one of the reasons. Figure 11, however, shows the fractional increase in I_{SiO_2} on removing the overlayers, so we may deduce the values of $I_{\text{SiO}_2}^{\infty}$ for wafers (1) and (2) as 681161 and 645925, respectively. Averaging these values and the two cited above gives

$$I_{\text{SiO}_2}^{\infty} = 673128 \pm 19648 \quad (R_o = 0.76) \quad (33)$$

In Part I¹ we calculated the carbon contamination level using the measured ratio I_C/I_{SiO_2} and the calculated ratio $I_C^{\infty}/I_{\text{SiO}_2}^{\infty}$ together with calculated values of the attenuation lengths $L_C(E_C)$ and $L_C(E_{\text{Si}})$. It is clear from Fig. 9 that we should be able to use Eqn (20) with the value of I_C^{∞} derived from Fig. 9(b) together with $L_C(E_C)$ in order to determine the contamination layer thickness. These results are shown as the abscissa in Fig. 12 compared with the earlier data from Part I¹ as ordinate for both glassy carbon and the average polymer. The ratios of the thickness of the carbonaceous contamination calculated from I_C/I_{SiO_2} from Part I¹ to that from I_C/I_C^{∞} here are 0.44 ± 0.02 for carbon as glassy carbon and 0.99 ± 0.05 for carbon as an average polymer. As seen above, the results are only consistent for carbon as described by an average polymer.

Bulk silicon dioxide

The value of R_o is very important but, as we have seen, the theoretical and experimental values given in Eqns (10) and

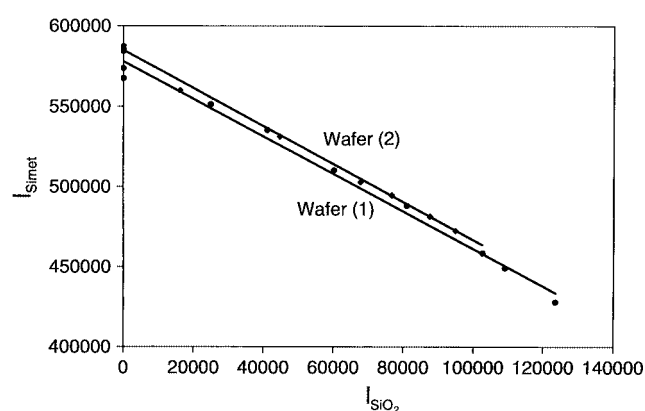


Figure 11. Variation of I_{SiO_2} versus I_{SiO_2} during sputter depth profiling of: (●) wafer (1) with $d_{\text{oxide}} = 0.733 \text{ nm}$; (◆) wafer (2) with $d_{\text{oxide}} = 0.531 \text{ nm}$. The solid lines are the least-squares fits to the data. Note that these intensities are reduced compared with the data given elsewhere in this work, as explained in the text.

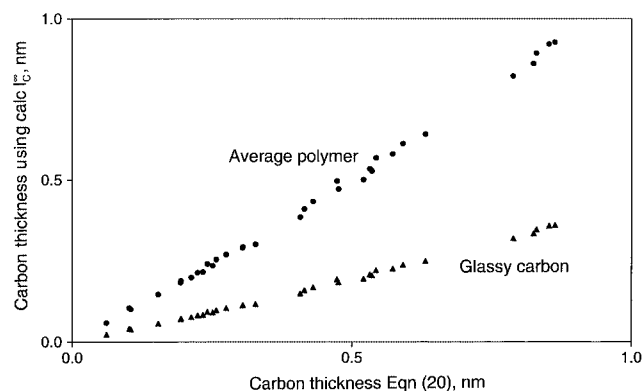


Figure 12. The carbon overlayer thickness derived from Eqn (20) as abscissa and from Eqns (9) and (10) of Part I¹ as ordinate.

(11) differ by a factor of 1.43. Moreover, the experimental data in this work from Fig. 11 indicate that R_o (experiment) is even higher than found in previous work and that the discrepancy between experiment and theory may be even greater. Generally, as we have seen, there are difficulties in measuring both I_{Si}^{∞} and $I_{\text{SiO}_2}^{\infty}$, which arise from the carbonaceous contamination. However, Fig. 9, giving the data for the Si 2p peak as a function of the carbon level, indicates that data may be extrapolated to a clean surface. We have therefore analysed both sides of two samples of a polished single-crystal SiO_2 and one of a thick thermal oxide, after cleaning with an overnight soak in isopropyl alcohol (IPA) or with a light rub with cotton wool soaked in ethanol followed by a carbon dioxide snow jet and an argon jet with a repeat of the last two procedures. In Part I¹ these were found to be among the most effective cleaning methods that did not affect the substrate.

The Si 2p and O 1s intensities as a function of the C 1s intensity from these cleaned and more contaminated states are given in Fig. 13. The divergence between the mean Si 2p intensities for the single-crystal SiO_2 and for the thermal oxide is 4.5% of the absolute intensities, with the $I_{\text{SiO}_2}^{\infty}$ (single crystal) being 585665 ± 33844 and $I_{\text{SiO}_2}^{\infty}$ (thermal oxide) being 612020 ± 16391 . Here the scatters are the standard deviations of eight and four results, respectively. In terms of the

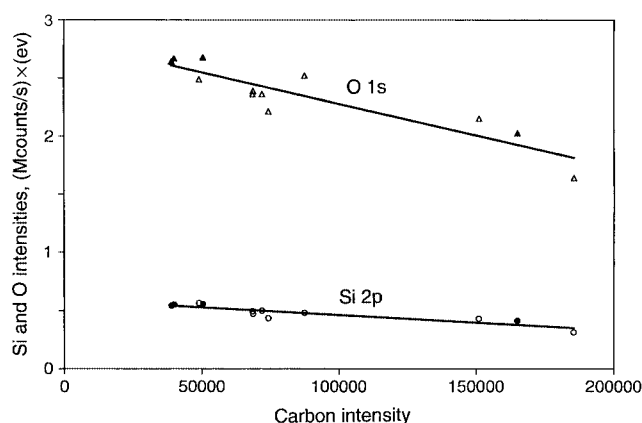


Figure 13. The Si 2p and O 1s intensities from single-crystal SiO_2 (open symbols) and for a thick thermal oxide (filled symbols) as a function of the C 1s intensity.

standard deviations of the means, these uncertainties fall to ± 11966 and ± 8196 , which do not encompass the separation of 51418. Hence

$$I_{\text{SiO}_2}^{\infty} (\text{single crystal}) = (0.957 \pm 0.023) \times I_{\text{SiO}_2}^{\infty} (\text{thermal oxide}) \quad (34)$$

Thus, we see a significant difference between these two samples in their Si 2p absolute intensities. However, the difference between the average values for the O1s/Si2p intensity ratios of these two oxides is 1.6%, where the standard deviation of this mean difference is 2.1%. We therefore conclude that the surfaces of the α -quartz and the thermal oxide are effectively of the same stoichiometry. However, the absolute bulk intensities differ. For a given material, these intensities depend linearly on the density, ρ , directly from N (see, for instance, Eqn (3)). This is cancelled by part of the inverse effect from the IMFP arising, in equation TPP-2M,³⁴ from the term E_p^{-2} , which is proportional to ρ^{-1} . There is a further term β^{-1} , which is complicated but, for SiO₂, the increase in density from 2.196 to 2.648 g cc⁻¹ would lead to a final fall in $I_{\text{SiO}_2}^{\infty}$ by a factor of 0.910. The change of 0.957 ± 0.023 seen lies between the results using the density of α -quartz and those of the thermal oxide, so we conclude that the ultrathin SiO₂ layers have a lower density than α -quartz as far as XPS is concerned but that the density may not be as low as 2.196 g cc⁻¹.

From the above $I_{\text{SiO}_2}^{\infty}$ (thermal oxide) data we deduce that

$$\frac{I_{\text{SiO}_2}^{\infty}}{I_{\text{Si metal}}^{\infty}} = 0.87 \pm 0.03 \text{ for } R_0 = 0.53 \quad (35)$$

$$\frac{I_{\text{SiO}_2}^{\infty}}{I_{\text{Si metal}}^{\infty}} = 0.91 \pm 0.02 \text{ for } R_0 = 0.76 \quad (36)$$

The two values arise from the two different R_0 values used to calculate some of the $I_{\text{Si metal}}^{\infty}$ values. Clearly, the second value is, internally, the more consistent because the ratio we are determining is, itself, an experimental value of R_0 . These values are close to the value of 0.85 ± 0.01 deduced in the sputtering study. The above and the sputtering study are independent in their approach and their agreement indicates that the experimental values are valid. The average of these two values, 0.88 ± 0.03 , is close to that of Fulghum^{17,18} and lies at the upper end of the range given by others in Table 2. It is very different from the theoretical value. In the previous section there were indications that the oxide may be more dense than the 2.196 g cc⁻¹ value and the density could be intermediate between 2.196 and 2.648 g cc⁻¹ of α -quartz. If the latter value is used to calculate R_0 from Eqn (4), the R_0 value increases, as noted before, from 0.53 to 0.64. This is insufficient to explain the observations given above and so, if Eqns (3) and (4) are valid the factor of 1.4 divergence could arise from inaccuracies in the theoretical values of λ_{Si} and λ_{SiO_2} . We saw earlier that the theoretical values of λ_{Si} and L_{SiO_2} were $18 \pm 9\%$ too low and $8 \pm 18\%$ too high, respectively, when compared with the experimental data. Inclusion of these values into the calculated value for R_0 reduces that value further to 0.42 ± 0.09 , but increases the uncertainty. This uncertainty does not cover the experimental value for R_0 and still leaves a serious inconsistency between the calculated and measured values of R_0 .

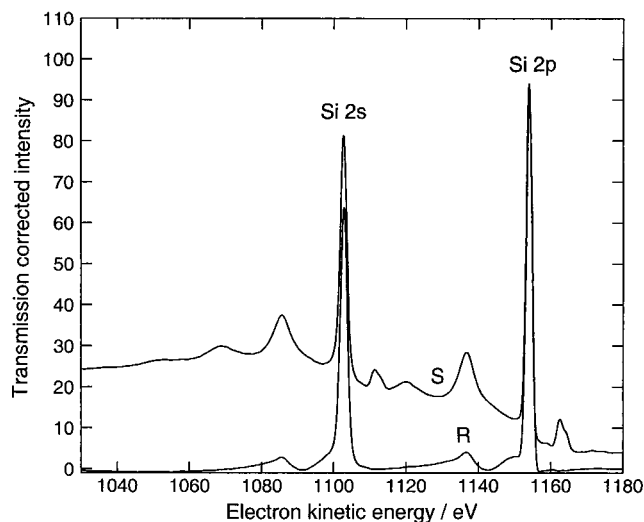


Figure 14. The XPS data for the Si 2p peaks using Mg x-rays: (S) true spectrum; (R) satellite and background-subtracted spectrum using deconvolution with the angle-averaged REELS data.³⁵

This inconsistency between the experimental and theoretical values of R_0 may arise from an inconsistency in the approaches used. The theoretical value relates to the total Si metal and total Si oxide intensities. The use of Shirley's background²⁸ is essential for the peak synthesis here but it removes all of the intrinsic shake-up intensity from the measurements. Recently we have developed a method of removing the extrinsic background from XPS peaks³⁵ using angle-averaged reflected electron energy-loss spectroscopy (REELS) data.³⁶ The Si 2p spectrum after correction for the spectrometer intensity/energy response function, and after satellite and REELS background subtraction, are given as S and R, respectively, in Fig. 14. From this we see that, for Si in the metallic state, the Shirley background only provides 80% of the intensity. This agrees with the predictions of Penn³⁷ and the data of Steiner *et al.*³⁸ for the series Na, Mg and Al. Much of the intrinsic intensity out of the peak appears in the first plasmon as a shake-up contribution. In SiO₂, the plasmon excitation is weaker and the Shirley background will recover a larger fraction of the true intensity. If, in the limit, it recovers all of the intensity, the calculated value of R_0 for the above measurement regime should be $0.53/0.80 = 0.66$ but if it only recovers the same fraction as for Si, then R_0 will remain at 0.53. This effect, together with uncertainties in λ_{Si} , λ_{SiO_2} and ρ_{SiO_2} , may explain the divergence between the theoretical and experimental values of R_0 and indicates why the calculated value of 0.53 is not to be recommended for use with Eqn (2). For analysis using Shirley's background and peak synthesis to deduce $I_{\text{Si metal}}$ and I_{SiO_2} and for use in Eqn (2), we recommend that R_0 be taken as 0.88 ± 0.03 . If this value is used to recalculate the data of Ebel *et al.*¹² and of Gross *et al.*¹³ for L_{SiO_2} in Table 3, the average value of L_{SiO_2} then rises to 0.984 of the theoretical value.

CONCLUSIONS

A study of the quantification issues has been made for analysis of the surface of ultrathin silicon dioxide layers

on Si. For practical applications involving analysis of the thickness of the oxide, a simple equation (Eqn (2)) is used with two parameters. The first of these, R_o , is the ratio of the Si intensities from pure bulk SiO_2 and pure bulk Si. The theoretical prediction for R_o , using the best current methods, gives a value of 0.53 ± 0.05 assuming that the SiO_2 density is 2.196 g cc^{-1} . Experimental data from the literature show a ratio of 0.76 ± 0.08 , which is incompatible with this. Extrapolation of experimental data for α -quartz and a thick thermal oxide as a function of contamination level to zero contamination shows that the thermal oxide has the same stoichiometry as the α -quartz but has a lower density consistent with the above density value. Measurements for R_o presented here give a value of 0.88 ± 0.03 by using thin oxides and bulk oxide samples corrected for contamination or by sputtering through an oxide layer. This value is at the high end of the range of experimental values previously reported and is not consistent with the theoretical value. This inconsistency may arise because the traditional method of peak synthesis leads to the measurement of slightly different areas to those used in the calculation. Additional effects occur through uncertainties in the parameters used in the theoretical prediction. For quantification from this work we therefore recommend the use of $R_o = 0.88 \pm 0.03$ with Eqn (2). For more accurate analysis, we need a set of careful measurements for samples with known thicknesses of oxide, established by independent methods, with defined traceabilities of 1% or better.

A detailed analysis of the effects of the measurement geometry show that diffraction effects can alter the effective value of R_o such that the deduced thickness may be in error by up to $\pm 20\%$. Conditions are defined for the analysis of thin oxides on (100) and (111) Si to minimize effects arising from the diffraction effects on the emission intensities of the Si 2p photoelectrons from the Si substrate. Here, a particularly good emission direction 'A' is found, well away from these intensity enhancements. For (100) surfaces this is at 34° from the surface normal in the azimuth at 22.5° to the [100] and [110] azimuths. For (111) surfaces 'A' is at 25.5° from the surface normal in the $[10\bar{1}]$ azimuth.

Finally, evaluation of the carbonaceous contamination also shows good consistency between the different calculational approaches, using either the calculated or experimental values of I_C^∞ , if data for an average polymer are used and not those for glassy carbon.

Acknowledgements

The authors would like to thank A. Chew and D. E. Sykes for the silicon wafers, J. E. Johnstone for HF etching of Si wafers, W. Unger for data relating to Ref. 13, C. J. Powell for drawing our attention to Ref. 22, D. A. Cole for data relating to Ref. 22 and P. Augustus for general advice on Si wafers. This work forms part of the Valid Analytical Measurement programme of the DTI National Measurement Systems Policy Unit.

REFERENCES

- Seah MP, Spencer SJ. *J. Vac. Sci. Technol. A*. to be published.
- Jablonski A. *Surf. Interface Anal.* 1989; **14**: 659.
- Kaye GWC, Laby TH. *Tables of Physical and Chemical Constants* (16th edn) Longman: Harlow, 1995.
- Lide DR. *CRC Handbook of Chemistry and Physics* (31st edn). CRC Press: Boca Raton, FL, 2000.
- Tanuma S, Powell CJ, Penn DR. *Surf. Interface Anal.* 1991; **17**: 911.
- Tanuma S, Powell CJ, Penn DR. *Surf. Interface Anal.* 1991; **17**: 927.
- Seah MP, Gilmore IS. *Surf. Interface Anal.* 2001; **31**: 835.
- Jablonski A, Powell CJ. *J. Vac. Sci. Technol. A* 1997; **15**: 2095.
- Powell CJ, Jablonski A. *J. Phys. Chem. Ref. Data* 1999; **28**: 19.
- Cumpson PJ, Seah MP. *Surf. Interface Anal.* 1997; **25**: 430.
- Powell CJ, Jablonski A. *J. Electron Spectrosc.* 2001; **114–116**: 1139.
- Ebel H, Ebel MF, Svagera R, Hofman A. *Surf. Interface Anal.* 1992; **18**: 821.
- Gross Th, Lippitz A, Unger W, Guttler B. *Surf. Interface Anal.* 2000; **29**: 891.
- Hill JM, Royce DG, Fadley CS, Wagner LF, Grunthaner FJ. *Chem. Phys. Lett.* 1976; **44**: 225.
- Ishizaka A, Iwata S, Kamigaki J. *Surf. Sci.* 1979; **84**: 355.
- Hochella MF, Carim AF. *Surf. Sci. Lett.* 1988; **197**: L260.
- Fulghum JE, Stokell R, McGuire GE, Patnaik B, Yu N, Zhao YJ, Parikh N. *J. Electron Spectrosc.* 1992; **60**: 117.
- Fulghum JE. *Surf. Interface Anal.* 1993; **20**: 161.
- Mitchell DF, Clark KB, Bardwell JA, Leonard WN, Mas-soumi GR, Mitchell IV. *Surf. Interface Anal.* 1994; **21**: 44.
- Yano F, Hiraoka A, Itoga T, Kojima H, Kanehori K, Mitsui Y. *J. Vac. Sci. Technol. A* 1995; **13**: 2671.
- Lu ZH, McCaffrey JP, Brar B, Wilk GD, Wallace RM, Feldman LC, Tay SP. *Appl. Phys. Lett.* 1997; **71**: 2764.
- Cole DA, Shallenberger JR, Novak SW, Moore RL, Edgell MJ, Smith SP, Hitzman CJ, Kirchhoff JF, Principe E, Nieveen W, Huang FK, Biswas S, Bleiler RJ, Jones K. *J. Vac. Sci. Technol. B* 2000; **18**: 440.
- Awaji N, Sugita Y, Nakanishi T, Ohkubo S, Takasaki K, Komiyama S. *J. Vac. Sci. Technol. A* 1996; **14**: 971.
- Richter CA, Nguyen NV, Dura JA, Majkrzak CF. *Characterisation for Metrology and ULSI Technology*, Seiler DG, Diebold AC, Bullis WM, Schaffner TJ, McDonald R, Walters EJ (eds). AIP: NY, 1998; 185.
- Ebel MF, Liebl W. *J. Electron Spectrosc.* 1979; **16**: 463.
- Seah MP. *J. Electron Spectrosc.* 1995; **71**: 191.
- Shirley DA. *Phys. Rev. B* 1972; **5**: 4709.
- Hollinger G, Himpsel FJ. *Appl. Phys. Lett.* 1984; **44**: 93.
- Himpsel FJ, McFeeley FR, Taleb-Ibrahimi A, Yarmoff JA. *Phys. Rev. B* 1988; **38**: 6084.
- Keister JW, Rowe JE, Kolodziej JJ, Niimi H, Tao H-S, Madey TE, Lucovsky G. *J. Vac. Sci. Technol. A* 1999; **17**: 1250.
- Egelhoff WF. *Crit. Rev. Solid State Mater. Sci.* 1990; **16**: 213.
- Chambers SA. *Surf. Sci. Rep.* 1992; **16**: 261.
- Han ZL, Hardcastle S, Harp GR, Li H, Wang XD, Zhang J, Tonner BP. *Surf. Sci.* 1991; **258**: 313.
- Tanuma S, Powell CJ, Penn DR. *Surf. Interface Anal.* 1994; **21**: 165.
- Seah MP, Gilmore IS, Spencer SJ. *Surf. Interface Anal.* 2001; **31**: 778.
- Seah MP. *Surf. Sci.* 2001; **471**: 185.
- Penn DR. *Phys. Rev. Lett.* 1977; **38**: 1429.
- Steiner P, Höchst H, Hüfner S. *Z. Phys. B* 1978; **30**: 129.